Optical and structural investigations of annealing impact on phase separation of Erbium-doped Al2O3 layers

N. Al Helou, L. Khomenkova, Emmanuel Cadel, Christophe Labbe, Julien Cardin, F. Gourbilleau, Etienne Talbot

Optical and structural investigations of annealing impact on phase separation of Erbium-doped Al_2O_3 layers

N. Al Helou [a], L. Khomenkova [b,c,d], E. Cadel [a], C. Labbé [b], J. Cardin [b], F. Gourbilleau [b], E. Talbot [a,*]

[a] Normandie Univ, UNIROUEN, INSA Rouen, CNRS, Groupe de Physique des Matériaux, 76000 Rouen, France
[b] CIMAP, CNRS, ENSICAEN, UNICAEN, CEA, Normandie Univ, 14050 Caen Cedex, France
[c] V. Lashkaryov Institute of Semiconductor Physics at the National Academy of Sciences of Ukraine, 45 Prospekt Naury, Kyiv 03028, Ukraine
[d] National university "Kyiv Mohyla academy", 2 Skovorody str., Kyiv 04070, Ukraine

ARTICLE INFO

Keywords:
Aluminum oxides
Cathodoluminescence
Phase transition
Structural properties
Rare-earth

ABSTRACT

We report on the effect of annealing treatment on the structural and optical properties of Er-doped Al_2O_3 thin films elaborated by atomic layer deposition. The properties of the films were studied using ellipsometry and Fourier-transform infrared (FTIR) spectroscopies, cathodoluminescence (CL) versus annealing temperature varied in the 650-1100 °C range. Spatial location and diffusion of chemical species were investigated at the atomic scale by atom probe tomography (APT). The CL measurements evidence Er^{3+} light emission over the visible-infrared spectral range. The CL spectra evolution showed non-monotonic variation with annealing temperature and a CL quenching occurring at 1000 °C. The CL signal evolution as a function of the annealing treatment is discussed regarding to the evolution of structural properties.

1. Introduction

In a growing global evolution in the electrical energy and renewable energy needs, the production of photovoltaic (PV) panels has grown considerably in recent decades. Significant researches have been done to increase the efficiency of silicon solar cells (Si-SC) which represent 90% of fabricated solar arrays. One of these research areas concerns the up-conversion approach (UC) to convert the incident solar light into a spectrum that matches the absorption of the active layer in solar cells, and hence to decrease a large proportion of losses and increase the solar cell efficiency [1]. This UC approach generally consists in converting two low-energy photons non-absorbed by the solar cell into one with higher energy photons before any absorption by the cell.

To date, considerable material fabrication work has been done on the growth and characterization of UC materials. Significant attention has been paid to metal ions embedded in inorganic hosts, mainly lanthanide- and transition metal ions [2–4]. One of the most efficient couple for up-conversion from near-infrared (NIR) to visible (VIS) spectral range was found to be Er^{3+}, Yb^{3+} [4,5]. Another, well-investigated NIR/VIS upconverter couple is Yb^{3+}/Tm^{3+} having $NaYF_4$ as a host material, which emits in the blue [4,6]. Transition metals have also been used for up-conversion such as: $Cs_2NaScCl_6:Pr^{3+};V^{3+}$ and $K_2NaScF_6:Er^{3+};V^{3+}$ [7] and Ti^{2+}, Ni^{2+}, Mo^{3+}, Re^{4+}, and Os^{4+} doped chloride and bromide host lattices [8]. Among the variety of materials, Er-doped Al_2O_3 is particularly an attractive candidate for up-conversion purposes due to the ability of Er ions to convert low energy photons to high energy photons, but also due to the high refractive index of the Al_2O_3 host material which is essential for the realization of waveguide type device [9]. More generally, Al_2O_3 is an interesting material for optical devices exhibiting a broad transparency from UV to IR and a high solubility for rare-earth dopants [10]. Moreover, it has recently been shown that $Er:Al_2O_3$ has great potential for silicon-based integrated photonic devices [11,12], luminescence enhancement [13, 14].

In this study, we used atomic layer deposition (ALD) to synthesize amorphous Al_2O_3:Er films on Si wafers. This approach is well known to allow the deposition of high-quality and uniform thin films. It has been extensively applied for the growth of Al_2O_3 coatings [15] and is used for the deposition of the Al_2O_3 passivation layer on the back of Si-SC. Thus Er^{3+} doping of Al_2O_3 host attracts great attention because of the possibility to extend the sensitivity of solar cells in the infrared spectral range. It was reported that the efficiency of such an up-conversion process depends strongly both on the Er^{3+} content and its spatial distribution inside the matrix [16].

To get insight into the evolution of Er-doped Al_2O_3 materials stimulated by thermal treatment, we have prepared Er-doped Al_2O_3 samples with the same Er content being annealed at different temperatures in the 650–1100 °C range. A detailed study of the effect of annealing

* Corresponding author.
E-mail address: etienne.talbot@univ-rouen.fr (E. Talbot).

https://doi.org/10.1016/j.mseb.2023.116672

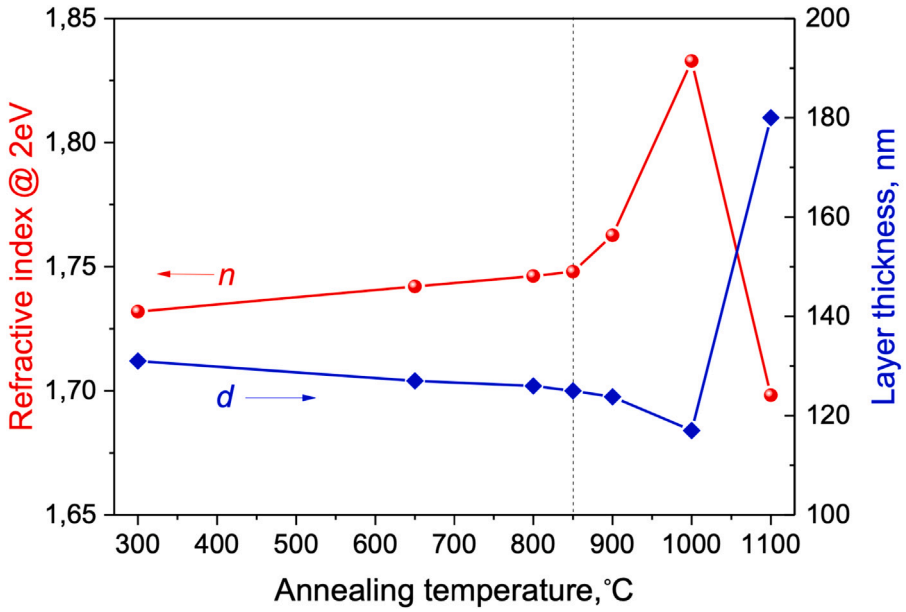

Fig. 1. Effect of annealing temperature on refractive index taken at 2.0 eV and thickness of the films.

temperature on the optical and structural properties of the Er-doped Al_2O_3 films is the goal of this work. The most attention is paid to the results obtained using the atom probe tomography and cathodoluminescence (CL). The former approach can provide a 3D chemical map of the sample at an atomic scale, allowing a very accurate and direct characterization of the distribution of Er ions inside Al_2O_3. The CL spectroscopy permits to study of the abundance of luminescence centers that existed in wide bandgap (about 8.9 eV) Al_2O_3 as well as to follow the evolution of light-emitting properties of native defects and dopants and its interrelation with films structure evolution at a nanoscale.

2. Experimental details

Er-doped Al_2O_3 films were grown in a Picosun 200 Advanced deposition tool [17]. Silicon wafers grown by Czochralski pulling technique produced by "Sil'tronix S.T". company were used as substrates [18]. These wafers were B-doped with (100) orientation. They were double-side polished and had 2 inches in diameter and 275±25 μm in thickness. Their resistivity was 15 Ω cm. The surface of virgin wafers was covered with a 5-nm thermal SiO_2 layer. To obtain Er-doped Al_2O_3 films the alternation of six Er_2O_3 and three Al_2O_3 cycles was used. The Er_2O_3 was grown using $Er(CpMe)_2$ as a precursor and distilled water as an oxidant. The bottle with $Er(CpMe)_3$ was heated at T_b = 160 °C. The pulse/purge durations of $Er(CpMe)_3$ were t_{pulse} = 1.6 s and t_{purge} = 2.0 s. The precursor- and boost-flows were 140 and 500 sccm, respectively. The water flow was 150 sccm and pulse/purge durations were fixed at t_{pulse} = 0.1 s and t_{purge} = 2.0 s. For Al_2O_3, the Trimethylaluminum (TMA) and water were used as precursors. The bottle with TMA was kept at T_b = 20 °C, the pulse/purge durations were t_{pulse} = 0.1 s and t_{purge} = 4 s, respectively. For H_2O, pulse and purge times were t_{pulse} = 0.1 s and t_{purge} = 6 s, respectively. The water container was kept at 20 °C during film deposition. The substrate temperature was T_d = 300 °C. After deposition, Si wafers were cut into small pieces (called hereafter as samples) and submitted to conventional thermal treatment at different temperatures, T_A, ranging from 650 to 1100 °C during t_A = 10 and/or 30 min in a nitrogen atmosphere.

The layers were investigated using spectroscopic ellipsometry using a Jobin-Yvon ellipsometer (UVISEL, HORIBA Ltd., Kyoto, Japan), where the incident light was scanned in the range of 1.5 to 6.0 eV under incident angles of 65, 70, and 75°. The beam spot was 1 mm in diameter. The spectra were recorded at the central point of each sample. The thickness of the films was about 130 nm being precisely controlled via the cycles' number. The factor of thickness non-uniformity was about 0.3%.

Fourier-transform infrared spectroscopy (FTIR) was carried out to follow the variation of film microstructure. The spectra were recorded at room temperature in the range of 450–4000 cm^{-1} using a Nicolet Nexus spectrometer under the normal incidence of the exciting light beam as well as under 60° incidence angle allowing registration of longitudinal optical phonons.

Cathodoluminescence (CL) was studied with a JEOL JSM-7900F scanning electron microscope (SEM) equipped with a HORIBA-HCLUE CL system. The CL spectra were acquired at room temperature with an accelerating voltage of the electron beam set to 6 kV and an electron beam current of 1.8nA. The light emitted by the sample under the impinging electron beam was collected by a parabolic mirror and sent to an IHR 320 (320 mm focal length) spectrometers for analysis in UV–Visible range with a 600 lines/mm grating (blazed at 500 nm). The signal is detected by a CCD camera Jobin-Yvon (UV–VIS range). The magnification used is 10000.

The spatial distribution of atoms was studied by atom probe tomography, which enables three-dimensional (3-D) elemental mapping of the analyzed volume with near-atomic resolution and high detection sensitivity [19]. APT specimens were prepared by lift-off method and annular milling of a focused ion beam using G4 PFIB CXe dual beam. To reduce Xe implantation and avoid damages in the region of interest, the Er -doped Al_2O_3 samples were capped with a layer of Pt, and a final polishing was performed at a low-acceleration voltage (12 kV). The samples were analyzed by laser-assisted wide-angle atom probe tomography (LAWATAP) from CAMECA. The analyses were performed in a high-vacuum chamber at 10^{-10} mbar at a temperature of 80 K using a femtosecond UV pulsed laser (λ = 343 nm) and a detector yield of 0.62. The APT data analyses were performed using the home built 'GPM3Dsoft' software.

3. Results and discussion

3.1. Ellipsometry and FTIR data

Fig. 1 displays the optical characterization of the films carried out using spectroscopic ellipsometry. At 2.0-eV detection energy, it was discovered that the refractive index of the films, both as-deposited and

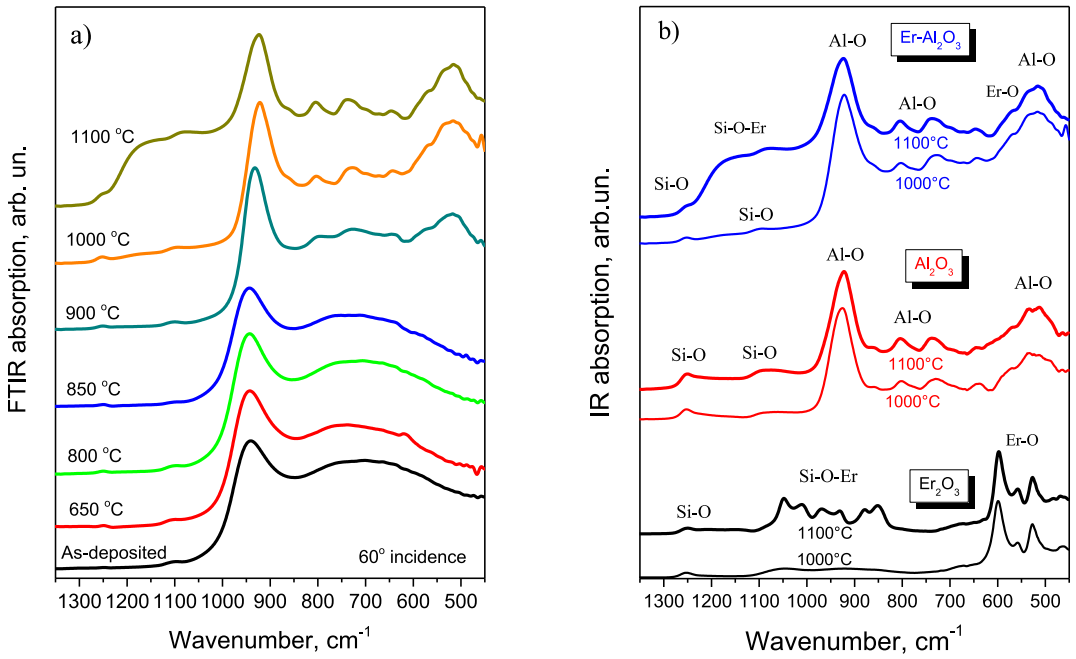

Fig. 2. FTIR spectra for Er-doped Al_2O_3 films (a) and pure Al_2O_3, pure Er_2O_3 and Er-doped Al_2O_3 films annealed at different T_A. The spectra were recorded with 60° incidence of excitation light. Annealing temperatures are mentioned in the figures. The spectra were shifted vertically for clarity.

annealed at $T_A \leq 650$ °C, was $n = 1.732 \pm 0.001$. With annealing, the films' thickness remains constant (130 nm). The refractive index rises to 1.748 and the thickness falls to d =125 nm as T_A rises from 650 to 850 °C. n increases up to 1.832 and d falls to 117 nm due to the densification of the amorphous phase during a heat treatment at T_A = 900–1000 °C. Last but not least, annealing at T_A = 1100° had the opposite effect, decreasing n to 1.695 and thickening the films (d = 180 nm). While the reduction of the refractive index observed at the maximum annealing temperature can be attributed to the formation of specific phases with low n within the films, such a transformation of the film characteristics allows for the expectation of crystallization of the films for T_A = 850-1100 °C. The latter can consist of voids or cavities as well as silicon-rich phases due to the diffusion of Si into the film volume from the substrate. We previously reported a comparable outcome for Er_2O_3 films produced using the same ALD strategy [20]. It was demonstrated that Si diffusion toward the film surface was controlled by the mismatch between the lattice parameter of the film and substrate. The FTIR spectra were acquired for the same samples to provide insight into the variation of the optical properties of the films in the current study.

Fig. 2 displays the FTIR spectrum of as-deposited film with the presence of vibration bands in the 500–1050 cm^{-1} related to Al-O vibration bands (Fig. 2). The most intense peaks observed are peaking at 710–720 cm^{-1} and 945 cm^{-1} and can be ascribed to transverse optical (TO) and longitudinal optical (LO) phonons of amorphous Al_2O_3 respectively. Annealing at $T_A \leq 850$ °C did not lead to the transformation of these FTIR spectra and therefore, in correlation with the evolution of the refractive index described above, testifies to the amorphous structure of such films.

Heating at higher T_A (> 850 °C) stimulates the appearance of several peaks in the 450–900 cm^{-1} range (Fig. 2). It can be seen that for T_A = 850–1100 °C, sharper TO peaks at 514, 575, 643, 738 and 804 cm^{-1} appear. Additionally, the LO peak near 945 cm^{-1} ($T_A \leq 850$ °C) moves to 931 cm^{-1} (T_A = 900 °C) and 923 cm^{-1} (T_A = 1000 °C) down to 921 cm^{-1} (T_A = 1100 °C). The assignment of all these peaks can be performed based on the comparison of the evolution of FTIR spectra of pure Al_2O_3 and pure Er_2O_3 films grown with the same ALD tool (Fig. 2,b) as well as on their comparison with the literature data [21]. As a result, γ–Al_2O_3 phase formation is stimulated by annealing at T_A = 850–1000 °C. Furthermore, taking into account the short annealing time (30 min), one can assume a very low contribution of θ– and δ–Al_2O_3 phases, if any. With further T_A rise up to 1100 °C, an appearance of α–Al_2O_3 phase can be expected [21]. Since no additional peaks appear in the FTIR spectra of the samples annealed at 1100 °C, one can assume the main contribution in these spectra is given by the γ–Al_2O_3 phase. This assumption is supported by the observation of the effect of SiO_2 addition into Al_2O_3 materials demonstrating the retarding of the formation of α–Al_2O_3 phase [22] that usually appears at $T_A \geq 1100$ °C [20]. However, FTIR spectra of such samples demonstrate additional vibration bands with the maxima near 1256, 1090, and 820 cm^{-1} (at T_A = 1000–1100 °C) that are the features of Si-O vibrations [20].

The comparison of FTIR spectra of pure Al_2O_3 and pure Er_2O_3 films (Fig. 2,b) allows assuming that the formation of Si-O-Er vibration bands also occurs. These latter can be explained by the formation of a SiO_x interfacial layer as well as by the diffusion of Er towards film/substrate interface and/or Si diffusion into film volume towards its surface. Similar behavior was reported by us earlier for the Er_2O_3 films grown on Si substrates with the same ALD approach [20]. These findings are in agreement with the ellipsometry data.

3.2. *Cathodoluminescence*

An evolution of light-emitting properties of the samples described above was investigated using CL spectroscopy. We have used this approach to excite all the emitting centers and to follow their light emission as a function of the annealing temperature. It should be noted that for Er-doped Al_2O_3 films only Er^{3+} related CL emission was registered contrary to defect-related Al_2O_3 emission observed for pure alumina films (not shown here). Fig. 3,a presents the CL spectra recorded in the 300–1000 nm spectral range for as-deposited samples and those annealed at 650–1100 °C. It was found that whatever T_A value, a CL signal originates from Er^{3+} ion intra-4f transitions is detected. The associated transitions for these recorded peaks are mentioned in the energy diagram in Fig. 3.b.

The characteristic doublet with the highest intensity is located at 548–558 nm range and can be assigned to the $^4S_{3/2} \rightarrow ^4I_{15/2}$ transition as reported by Brien et al. for AlNOEr films [23]. Other dominant

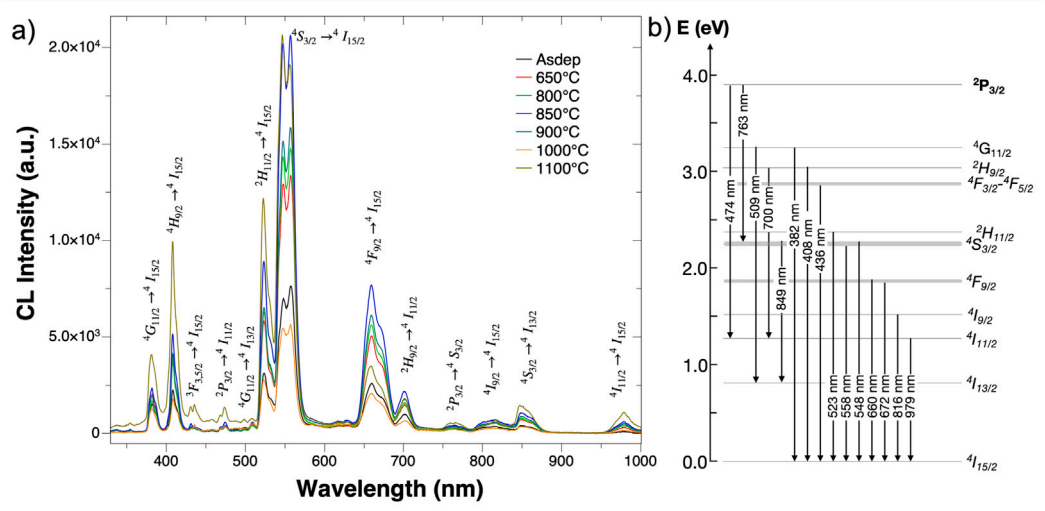

Fig. 3. (a) CL spectra in the UV–Visible range for the Er-doped Al_2O_3 sample annealed at different temperatures. (b) Schematic presentation of intra-4f shell of Er^{3+} ions.

transitions can be distinguished at 382 nm, 408 nm, 523 nm, and 660 nm and are attributed to radiative relaxation from different excited states of Er^{3+} ions to the $^4I_{15/2}$ ground state. For the transitions from $^4S_{3/2}$, $^4F_{9/2}$, $^4I_{11/2}$ states to the $^4I_{15/2}$ level, we can notice the presence of broad and inhomogeneous emission CL bands. The latter transition may be of particular interest since most of Er-based solid state lasers are pumped through this energy level [24]. Such a broadening can be related to local effects on the splitting of band structure levels resulting from high disorder in crystalline or amorphous materials where Er atoms encounter different local environments [25]. Moreover, in most of the oxides, the transition from the $^4I_{9/2}$ level of Er^{3+} ion is quenched by multiphonon relaxation and appears as very weak [24]. We find no discernible relationship between annealing temperature and the emergence or disappearance of CL peaks. However, we can notice an enhancement of the $^4S_{3/2} \rightarrow ^4I_{15/2}$ doublet intensity for an annealing at 1100 °C (Fig. 3.a). It is well known that rare-earth transitions are sensitive to the local environment of ions and can be used as "markers" of an evolution of the microstructure at the nanoscale with the annealing temperature. In the present case, the observe evolution of the CL spectra as function of annealing temperature does not allow to evidence a structural evolution.

In the following, we will concentrate our intention on the Er luminescence bands evolution. With the annealing temperature, the luminescence depends on the ion distribution in the matrix, its concentration as well as on the microstructure of the sample. The modifications in the CL spectra are related to the settlement of the excited states in Er^{3+} ions. The distribution of the CL intensity is due to the competing ways of achieving excited states in erbium ions.

Fig. 4 presents the annealing temperature dependence of the integrated CL intensity. Integration was performed either on the whole wavelength range (300–1000 nm) or by considering specific regions. The wavelength ranges 375–395 nm, 400–420 nm, 515–536 nm, 536–576 nm, 640–689 nm, and 954–1000 nm correspond to $^4G_{11/2} \rightarrow ^4I_{15/2}$, $^2H_{9/2} \rightarrow ^4I_{15/2}$, $^2H_{11/2} \rightarrow ^4I_{15/2}$, $^4S_{3/2} \rightarrow ^4I_{15/2}$, $^4F_{9/2} \rightarrow ^4I_{15/2}$, $^4I_{11/2} \rightarrow ^4I_{15/2}$ transitions', respectively. The evolution follows the same trend independently of the emission band. We can distinguish three different regimes as a function of annealing temperature.

From as-deposited to 850 °C, the integrated CL of the all-emission bands increases before decreases and reaches a minimum at 1000 °C from 850 °C to 1000 °C. Finally, for the highest annealing temperature, the integrated CL intensity increases. It is noteworthy that the increase of intensity of the 640–689 nm bands, related to the $^4F_{9/2} \rightarrow ^4I_{15/2}$ transition, is weaker than the others bands.

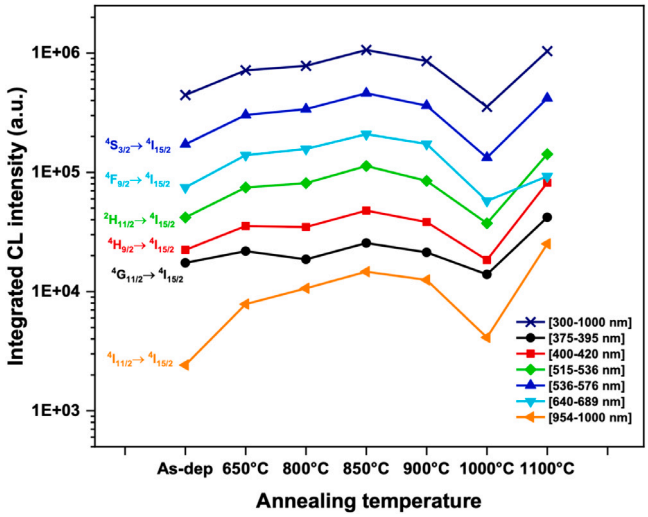

Fig. 4. Integrated CL intensities as a function of the annealing temperature for selected optical Er^{3+} transitions.

The state $^4F_{9/2}$ may arise as a result of energy transfer from a nearby excited erbium, as well as $^4F_{7/2} + ^4I_{11/2} \rightarrow 2^4F_{9/2}$ cross-relaxation (CR).

As the annealing temperature rises, favoring an increase in the spacing between the Er^{3+} ions, the intensity of the green band (520 nm) increases while the red band decreases, which is consistent with the absence of the excited state $^4F_{9/2}$ [26]. The CR process, which generates the excited state $^4F_{9/2}$, causes the luminescence, which peaks at 660 nm.

A similar evolution of the luminescence has been previously observed in Ce-doped silicon-rich silicon oxide by Weimmerskirch-Aubatin et al. [27] and by Li et al. [28] and has been ascribed to an evolution of the location of dopants by Beainy et al. [29]. Ce atoms, firstly form aggregates with Si atoms leading to the quenching of the luminescence, before diffusing with the annealing temperature favoring the growth of Cerium silicate nanoparticles that are responsible of the re-appearance of an intense luminescence [29]. In the case of Al_2O_3 matrix doped with Er ions, such an evolution is not reported in the literature and the precise origin of the quenching at 1000 °C should be investigated.

Considering the first regime ($T_A \leq 850$ °C), the increase of CL is related to the decrease of non-radiative recombination centers coming

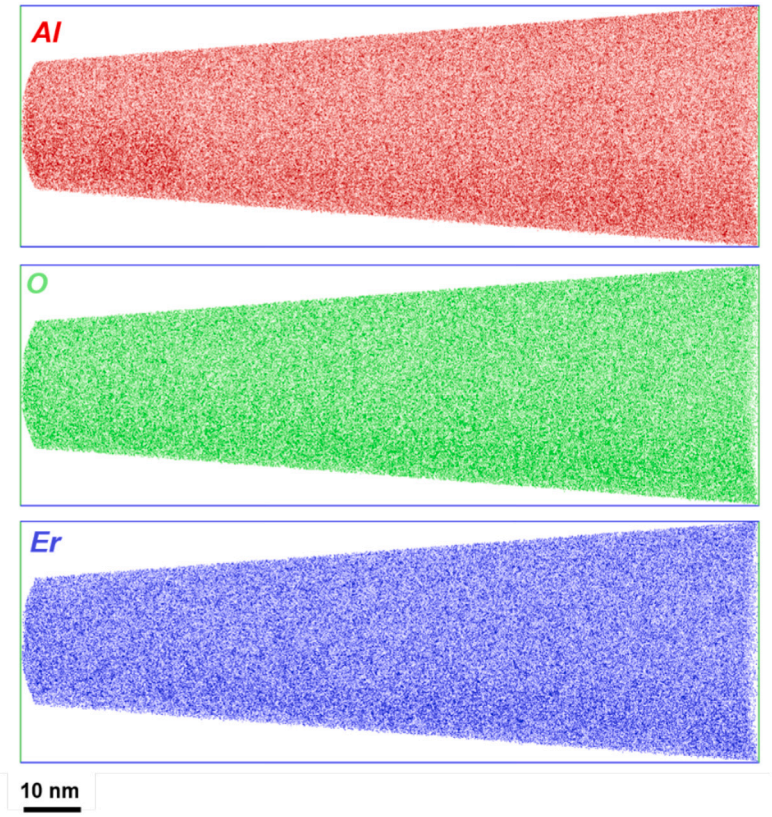

Fig. 5. 3-D reconstructions volume of APT analysis of the sample annealed at 650 °C, Al atoms are represented in red color, O in green, and Er in blue. (Volume: $42\times42\times126 nm^3$).

from the recovery of induced-growth defects. For the second regime (T_A = 850–1000 °C), the decrease of the CL intensity is attributed to the structural transformation and film densification resulting in the smaller distance between Er^{3+} ions. This can increase the probability of non-radiative recombination such as back energy transfer. Another reason for the quenching of Er^{3+} CL signal can be attributed to the Er^{3+} diffusion and precipitation during the annealing treatment [30] or to a modification of the valence of Er ions from 3+ to 2+ [31].

But it is quite surprising to observe an enhancement of the CL intensity for T_A = 1100 °C (the third regime). Meanwhile, the increase of the film thickness can increase the Er–Er distance and reduce non-radiative recombination probability, and, for instance, to change the CR processes of Er^{3+} ions [26]. To determine the nanostructure evolution with annealing treatment, atom probe tomography analyses have been performed for the samples submitted to annealing at 650 °C, 1000 °C, and 1100 °C.

3.3. Atom probe tomography

Fig. 5 shows 3-D reconstructions obtained Er-doped Al_2O_3 annealed at 650 °C, where the Er atoms are represented in blue color, Al in red, and O in green.

The APT analysis allows us to measure the composition of each element. The mean chemical composition has been determined from the mass spectrum and the proportions of atoms of each species. The mean content of aluminum, oxygen and erbium was found to be $X_{Al} = 36.8 \pm 0.2$ at.%, $X_O = 52.8 \pm 0.2$ at.%, $X_{Er} = 10.4 \pm 0.1$ at.% respectively. This reconstruction of the analyzed volume reveals that all the chemical atoms are homogeneously distributed even with the incorporation of high-content of Er in Al_2O_3, demonstrating the potentiality of such a growth technique. Similar analyses have been performed for the two other samples annealed at 1000 °C and 1100 °C.

The results allow us to compare the microstructure evolution and erbium location of the samples annealed at different temperatures. Fig. 6 represents cross-sectional views of the 3D reconstruction of the Er ions of the samples the annealed at 650 °C (Fig. 6.a), 1000 °C (Fig. 6.b), 1100 °C (Fig. 6.c). As mentioned previously, the sample annealed at 650 °C shows a random distribution of Er in the sample. Note that the as-deposited sample (not presented in this work) also shows a random distribution of the species inside the layer. At a first glance and as it can be seen in this Fig. 6, after being annealed at 1000 °C and 1100 °C, the sample shows an inhomogeneous distribution which amplifies with the temperature.

For a more precise study of the evolution of chemical species with the annealing treatment, the spatial distribution of the Al, O, and Er atoms was examined by the statistical test of homogeneity. Each dataset was divided up into equal blocks of 100 atoms. These distributions have been obtained by selecting the peaks corresponding to the aluminum (Al^{3+}, Al^{2+} and Al^{+} at 9, 13.5, and 27 u.m.a respectively in the mass spectrum), to the oxygen (O^{+} at 16 u.m.a.) and erbium (Er^{3+} and Er^{2+} at almost 55 and 83 u.m.a respectively). The corresponding frequency distributions of the atoms are presented in comparison to the random distribution of atoms in the analyzed volume. If the distribution of the atoms is random, the concentration frequency distribution will be represented by a binomial law. The comparison between the experimental distribution and the binomial law is carried out by the test of χ^2.

The χ^2 statistics also significance testing of the departure from randomness and the similarity between these two distributions.

Fig. 7 shows the frequency distribution of Al, O, and Er atoms for the three annealing conditions investigated by APT. Fig. 7.a reveals that the Al, O and Er atoms can be considered to be randomly distributed only in the Al_2O_3 sample annealed at 650 °C.

Even if it is not visually obvious in the atomic distribution (Fig. 5.b) of the sample annealed at 1000 °C, the distribution of Al and Er cannot be considered as randomized distribution (Fig. 6.b) where significant deviation from experimental and random distributions are noticed. However, O atoms distribution agrees with the binomial distribution.

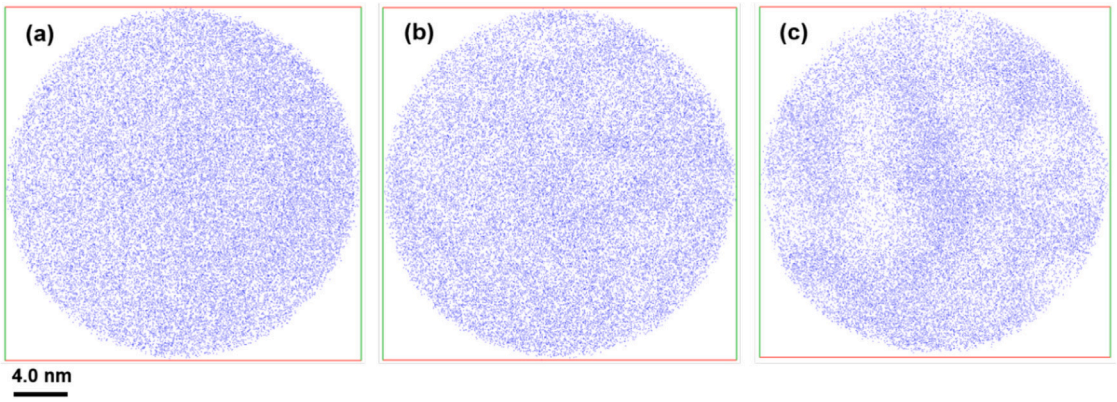

Fig. 6. 3D reconstruction of the Er ions in the annealed sample at (a) 650 °C, (b) 1000 °C, (c) 1100 °C.

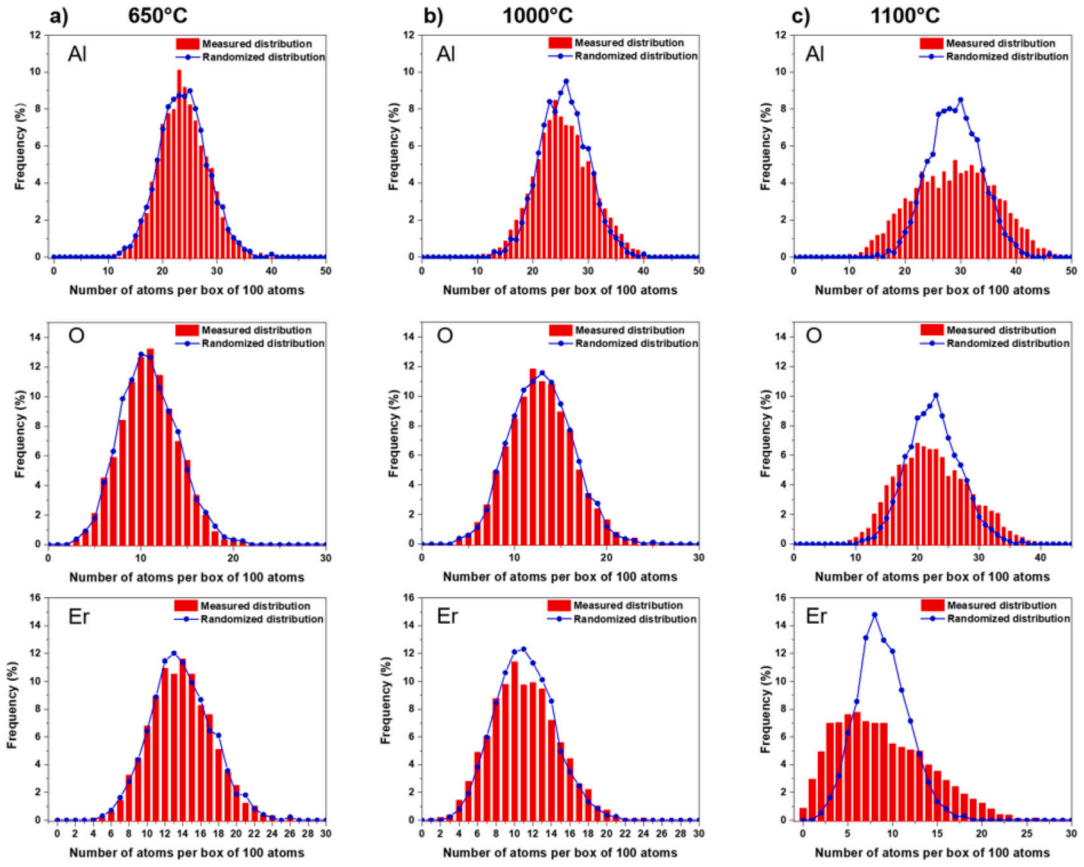

Fig. 7. Frequency distributions of Al, O and Er observed in the case of a distribution of 100 atoms in layers annealed at (a) 650 °C, (b) 1000 °C and (c) 1100 °C.

The experimental distribution of Al, O, and Er atoms for the sample annealed at 1100 °C (Fig. 7.c) can be seen to have widened and shifted in comparison to its corresponding randomized distribution. The significant shift away from the binomial law in the experimental distribution indicates that the atoms are arranged in a non-random manner related to the diffusion of species.

On the other hand, the spatial distribution of chemical species is modified with increasing annealing temperature. A slight deviation from the random case starting with Al and Er atoms at 1000 °C is observed, indicating that probably Al and Er diffuse at a lower temperature than O.

To quantify more precisely the evolution of Er atoms in the structure, we have used the first nearest neighbor (1NN) distribution method. This method allows studying the distance distribution of dopants in a volume [32]. When we consider a model of 1NN distances in a system of a mixture of two phases α and β, the probability density $P(r)$ assembling the distribution of both phases could be written:

$$P(r) = (1 - f)P_{\alpha}(r) + f\,P_{\beta}(r) \tag{1}$$

Where f is the atomic fraction of 1NN pair in β phase and the intrinsic distributions ($P_i(r)$) of both phases α and β could be written as:

$$P_i(r) = 4\pi r^2 Q C_i . exp\left(-\frac{4}{3}\pi Q C_i r^3\right), \quad \mathrm{i} = \alpha \quad \text{and} \quad \beta \tag{2}$$

and

$$f = \frac{C_{\beta}}{C_0}\left(\frac{C_0 - C_{\alpha}}{C_{\beta} - C_0}\right), \tag{3}$$

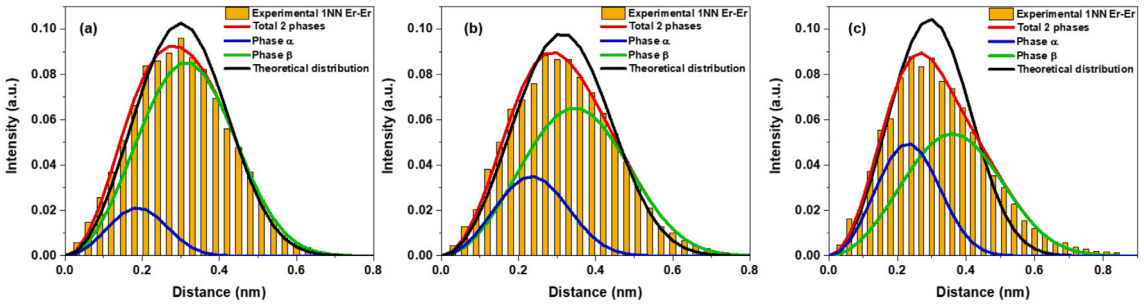

Fig. 8. Distribution of the first nearest neighbor distance between erbium atoms in sample annealed at 650 °C (a), 1000 °C (b) and 1100 °C (c).

where C_α and C_β are the compositions of the α and β phases respectively and C_0 is the overall composition. In a simplified form, the α phase deals with low distance and corresponds to 'aggregation' and the β phase with high distance corresponds to atoms diluted in the matrix.

The experimental distribution, computed from APT data, has been fitted with two components (Fig. 8): a 1NN distribution (blue line) describing the distribution of Er in the short-distance range (phase α) and a 1NN distribution (green line) describing the distribution of Er in the long-distance range (phase β). The 1NN distribution corresponding to the case of homogeneous distribution is represented (black line) for comparison. The position of the peaks for each of the two distributions represents the most probable distance of atoms of Er first neighbors in the first and second phase respectively.

To follow the evolution of the spatial distribution of the Er atoms as a function of the annealing temperature, we have applied this statistical method on the same three samples (annealed at 650 °C, 1000 °C, and 1100 °C) (Fig. 8). In the case of the sample annealed at 650 °C, the distribution of Er atoms exhibits a slight deviation from an uniform distribution. 1NN curve can be fitted with "two phases" where Er ions are mostly at two different distances. There are determined, by extraction from the 1NN distribution, to be 0.18 and 0.3 nm for α and β phases respectively. It should be noted that the intensity of the β phase is much more important than the intensity of α one.

The Er:Al_2O_3 films annealed at 1000 °C show more pronounced separation of two phases on the 1NN distributions (Fig. 8.b). A fraction (27%) of Er atoms is at the mean distance of about 0.24 nm (phase α) from each other and the other part (73%) at the distance of 0.36 nm (phase β). α phase is still the more important in the sample annealed at 1000 °C. The 1NN approach for the sample annealed at 1100 °C reveals a more pronounced non-uniform distribution of Er atoms as already evidenced in frequency distribution (Fig. 5.c). The two observed phases show the same atomic distances as the sample annealed at 1000 °C: 0.24 and 0.36 nm for α and β phases respectively but with a quasi-equal intensity for both distributions. This effect indicates an increase of the α phase with annealing temperature which can be related to the diffusion of Er atoms and is a sign of the first stage of Er segregation in the Al_2O_3 matrix.

The results of the 1NN approach are consistent with frequency distribution analysis. The thermal annealing activates the phase separation between Al, O and Er elements. Thus, considering all the observations extracted from APT analyses; it is obvious that the diffusion mechanism is activated by annealing, at the first, for Al and Er atoms and, afterwards, for O atoms. No formation of clusters or secondary phases has been detected. There is, therefore, a creation of local inhomogeneity of Er with the increasing stages of annealing. The evolution of chemical species location can be correlated to the CL emission observed (Fig. 3.a).

The first stage of CL intensity increases (up to 850 °C), dealing with homogeneous distribution of all elements, especially Er ions, in the Er:Al_2O_3 layer. It can be associated with recovering of growth defects and densification of the film such as the O vacancy defects originally present in the sample that may have been removed by the annealing treatment [33]. Also, the increase of the Er-related luminescence can partially be explained by the formation of Er–O complexes that appear after annealing. In fact, Er^{3+} ions are optically activated by these Er–O complexes [34].

The decrease of CL emission observed for electronic transitions starting from 850 °C up to 1000 °C, can be explained by the formation of Er-rich inhomogeneities at the nanometer scale as evidenced by APT (Fig. 6.b). The observed Er diffusion during annealing occurs in the same time that the evolution of the Al_2O_3 matrix from amorphous to crystalline γ phase. Cattaruzza et al. have shown, using XRD measurements, in Er:Al_2O_3 films deposited by radiofrequency magnetron co-sputtering that annealing treatments lead to the formation of erbium aluminates such as $ErAlO_3$ [35]. The formation of erbium composite can determine a local increase of the Er concentration. The mean distance between dopant ions is much shorter so that they could interact by an electric multipolar process leading to energy migration and consequently, to a luminescence intensity decrease due to the concentration quenching effect. Despite the few studies on alumina, it is known that the alumina matrix does not act in a similar way to silica [36]. The concentration quenching of RE doped silica is often attributed to the agglomeration of RE ions which is hard to observe in an alumina matrix with usual characterization techniques. Although, clustering on an atomic scale could not be ruled out due the to small local atomic arrangement. It has also been shown that the high-temperature annealing could favor the formation of the theta phase and the erbium ions could act like impurities and enhance the formation of this phase. The formation of Er-rich zones evidenced by APT can be the first stage of formation of such a complex responsible of the decrease of CL.

Finally, the enhancement of emission beyond the annealing process at 1000 °C, more specifically for $4G_{11/2}$ and $4H_{9/2}$ to $4G_{15/2}$ transitions (at 382 and 408 nm) and for $4S_{3/2}$ and $4F_{11/2}$ to $4I_{15/2}$ (849 and 979 nm) have been associated with the increase Er-Er distance with the increase of the film thickness related to the formation of Er:SiO_x interfacial layer. The regions with a high Er concentration contain a low Al concentration whereas the oxygen content is quite constant. We cannot rule out a contribution of Er introduced in the interfacial layer to the increase of CL intensity. However, it is well established that the solubility of Er ions in silicon oxide is low (< 0.1 at.%) so that one can expect a minor of this Er amount in the CL signal.

Up-conversion measurements have been realized on the Er doped Al_2O_3 layers for all annealing temperatures. UC process has not been demonstrated in this study which can be explained by the difficulty to manage Er-Er distance.

4. Conclusion

The structural and optical properties of Er-doped Al_2O_3 thin films elaborated by atomic layer deposition were investigated using ellipsometry, FTIR, APT, and CL methods. The results evidence that ALD techniques allow to fabricate high concentration and homogeneous Er doped Al_2O_3 thin layer. It has been shown that the annealing

temperature enables the control of amorphous or crystalline Al_2O_3 thin films without concentration quenching effect on luminescence. High cathodoluminescence intensity is obtained both in amorphous sample annealed at 850 °C or crystalline one after 1100 °C thermal treatment. The post-grown annealing initiates the diffusion of each chemical species leading to an inhomogeneous distribution of Er^{3+} ions. The Er^{3+} cathodoluminescence has the lowest intensity in the films annealed at 1000 °C and was explained by the clustering of Er-ions. At higher temperatures (1100 °C) an enhancement of Er CL emission was observed and was attributed to an increase of Er–Er distance and decrease of non-radiation recombination contribution.

Declaration of competing interest

The authors declare that they have no known competing financial interests or personal relationships that could have appeared to influence the work reported in this paper.

Data availability

Data will be made available on request.

Acknowledgments

This work was supported by the Normandie Region and the "Fond Européen de Développement Régional" (FEDER) via LUMIERE project. This work was partially supported by the CNRS Federation IRMA - FR 3095.

References

[1] V. Badescu, A.M. Badescu, Improved model for solar cells with up-conversion of low-energy photons, Renew. Energy 34 (6) (2009) 1538–1544, http://dx.doi.org/10.1016/j.renene.2008.11.006.

[2] G. Blasse, B.C. Grabmaier, A general introduction to luminescent materials, in: Luminescent Materials, Springer Berlin Heidelberg, Berlin, Heidelberg, 1994, pp. 1–9, http://dx.doi.org/10.1007/978-3-642-79017-1_1.

[3] F. Auzel, Upconversion and anti-Stokes processes with f and d ions in solids, Chem. Rev. 104 (1) (2004) 139–174, http://dx.doi.org/10.1021/cr020357g.

[4] J.C. Goldschmidt, S. Fischer, Upconversion for photovoltaics – A review of materials, devices and concepts for performance enhancement, Adv. Opt. Mater. 3 (4) (2015) 510–535, http://dx.doi.org/10.1002/adom.201500024.

[5] N. Menyuk, K. Dwight, J.W. Pierce, NaYF4 : Yb,Er—An efficient upconversion phosphor, Appl. Phys. Lett. 21 (4) (1972) 159–161, http://dx.doi.org/10.1063/1.1654325.

[6] J.F. Suyver, J. Grimm, M.K. van Veen, D. Biner, K.W. Krämer, H.U. Güdel, Upconversion spectroscopy and properties of NaYF4 doped with Er3+, Tm3+ and/or Yb3+, J. Lumin. 117 (1) (2006) 1–12, http://dx.doi.org/10.1016/j.jlumin.2005.03.011.

[7] C. Reinhard, K. Krämer, D.A. Biner, H.U. Güdel, V3+ sensitized upconversion in Cs2NaScCl6:Pr3+;V3+ and K2NaScF6:Er3+;V3+, J. Alloys Compd. 374 (1) (2004) 133–136, http://dx.doi.org/10.1016/j.jallcom.2003.11.068.

[8] D.R. Gamelin, M. Wermuth, H.U. Güdel, Up-conversion processes of 5d transition metal ions in crystals, J. Lumin. 83–84 (1999) 405–410, http://dx.doi.org/10.1016/S0022-2313(99)00134-9.

[9] G. Dingemans, A. Clark, J.A. van Delft, M.C.M. van de Sanden, W.M.M. Kessels, Er3+ and si luminescence of atomic layer deposited Er-doped Al2O3 thin films on Si(100), J. Appl. Phys. 109 (11) (2011) 113107, http://dx.doi.org/10.1063/1.3595691.

[10] W.A.P.M. Hendriks, L. Chang, C.I. van Emmerik, J. Mu, M. de Goede, M. Dijkstra, S.M. Garcia-Blanco, Rare-earth ion doped Al2O3 for active integrated photonics, Adv. Phys.: X 6 (1) (2021) 1833753, http://dx.doi.org/10.1080/23746149.2020.1833753.

[11] K. Yuan, L. Yang, Y. Yang, J. Sun, Improvement of the electroluminescence performance from Er-doped Al2O3 nanofilms by insertion of atomic Ga2O3 layers, Appl. Phys. Lett. 119 (20) (2021) 201105, http://dx.doi.org/10.1063/5.0064221.

[12] J. Rönn, W. Zhang, A. Autere, X. Leroux, L. Pakarinen, C. Alonso-Ramos, A. Säynätjoki, H. Lipsanen, L. Vivien, E. Cassan, Z. Sun, Ultra-high on-chip optical gain in erbium-based hybrid slot waveguides, Nature Commun. 10 (1) (2019) 432, http://dx.doi.org/10.1038/s41467-019-08369-w.

[13] J. Rönn, L. Karvonen, C. Kauppinen, A.P. Perros, N. Peyghambarian, H. Lipsanen, A. Säynätjoki, Z. Sun, Atomic Layer Engineering of Er-Ion Distribution in Highly Doped Er:Al2O3 for Photoluminescence Enhancement, ACS Photonics 3 (11) (2016) 2040–2048, http://dx.doi.org/10.1021/acsphotonics.6b00283.

[14] J. Zhu, B. Zhang, Y. Huang, Z. Lv, L. Ying, Y. Mei, Z. Zheng, D. Zhang, Optical gain at 1.55 μm of Er(TMHD)3 complex doped polymer waveguides based on the intramolecular energy transfer effect, Opt. Express 31 (4) (2023) 5242–5256, http://dx.doi.org/10.1364/OE.479180.

[15] S.M. George, Atomic layer deposition: An overview, Chem. Rev. 110 (1) (2010) 111–131, http://dx.doi.org/10.1021/cr900056b.

[16] A. Polman, Erbium implanted thin film photonic materials, J. Appl. Phys. 82 (September 1996) (1997) 1–39.

[17] PICOSUNTM, R-series Atomic Layer Deposition (ALD) reactors, URL https://www.picosun.com/product/r-200-advanced/.

[18] URL https://www.sil-tronix-st.com/en/silicon-wafer/silicon-wafer-specifications.

[19] W. Lefebvre-Ulrikson, F. Vurpillot, X. Sauvage (Eds.), Front matter, in: Atom Probe Tomography, Academic Press, 2016, p. iii, http://dx.doi.org/10.1016/B978-0-12-804647-0.01001-9.

[20] L. Khomenkova, M.-P. Chauvat, P. Marie, C. Frilay, F. Lemarié, S. Boudin, X. Portier, N. Ratel-Ramond, C. Labbé, J. Cardin, F. Gourbilleau, Thermally induced evolution of optical and structural properties of Er2O3 films grown on si substrates by thermal atomic layer deposition, Mater. Lett. 263 (2020) 127216, http://dx.doi.org/10.1016/j.matlet.2019.127216.

[21] A. Boumaza, L. Favaro, J. Lédion, G. Sattonnay, J.B. Brubach, P. Berthet, A.M. Huntz, P. Roy, R. Tétot, Transition alumina phases induced by heat treatment of boehmite: An X-ray diffraction and infrared spectroscopy study, J. Solid State Chem. 182 (5) (2009) 1171–1176, http://dx.doi.org/10.1016/j.jssc.2009.02.006.

[22] I. Koltsov, G. Kimmel, S. Stelmakh, K. Sobczak, W. Lojkowski, The new nano-enabled phase map of ZrO2-Al2O3, Sci. Rep. 9 (1) (2019) 5540, http://dx.doi.org/10.1038/s41598-019-42058-4.

[23] V. Brien, P.R. Edwards, P. Boulet, K.P. O'Donnell, Room temperature cathodoluminescence quenching of Er3+ in AlNOEr, J. Lumin. 205 (2019) 97–101, http://dx.doi.org/10.1016/j.jlumin.2018.09.012.

[24] T. Sanamyan, R. Pavlacka, G. Gilde, M. Dubinskii, Spectroscopic properties of Er3+-doped α-Al2O3, Opt. Mater. 35 (5) (2013) 821–826, http://dx.doi.org/10.1016/j.optmat.2012.10.036.

[25] K. Drdlíková, R. Klement, D. Drdlík, T. Spusta, D. Galusek, K. Maca, Luminescent Er3+ doped transparent alumina ceramics, J. Eur. Ceram. Soc. 37 (7) (2017) 2695–2703, http://dx.doi.org/10.1016/j.jeurceramsoc.2017.02.017.

[26] V.V. Halyan, I.A. Ivashchenko, Mechanism of photoluminescence in erbium-doped chalcogenide, in: S. Pyshkin (Ed.), Luminescence, IntechOpen, Rijeka, 2020, http://dx.doi.org/10.5772/intechopen.81445.

[27] J. Weimmerskirch-Aubatin, M. Stoffel, X. Devaux, A. Bouché, G. Beainy, E. Talbot, P. Pareige, Y. Fagot-Révurat, M. Vergnat, H. Rinnert, Observation of a nanoscale phase separation in blue-emitting Ce-doped SiO1.5thin films, J. Mater. Chem. C 3 (48) (2015) 12499–12506, http://dx.doi.org/10.1039/c5tc02722e.

[28] J. Li, O. Zalloum, T. Roschuk, C. Heng, J. Wojcik, P. Mascher, The formation of light emitting cerium silicates in cerium-doped silicon oxides, Appl. Phys. Lett. 94 (1) (2009) 011112, http://dx.doi.org/10.1063/1.3067871.

[29] G. Beainy, J. Weimmerskirch-Aubatin, M. Stoffel, M. Vergnat, H. Rinnert, C. Castro, P. Pareige, E. Talbot, Structural and optical study of Ce segregation in Ce-doped SiO1.5thin films, J. Appl. Phys. 118 (23) (2015) 234308, http://dx.doi.org/10.1063/1.4938061.

[30] A. Polman, D.C. Jacobson, D.J. Eaglesham, R.C. Kistler, J.M. Poate, Optical doping of waveguide materials by MeV Er implantation, J. Appl. Phys. 70 (1991) 3778, http://dx.doi.org/10.1063/1.349234.

[31] Y. Mebrouk, F. Mady, M. Benabdesselam, J.-B. Duchez, W. Blanc, Experimental evidence of Er3$+$ ion reduction in the radiation-induced degradation of erbium-doped silica fibers, Opt. Lett. 39 (21) (2014) 6154–6157, http://dx.doi.org/10.1364/OL.39.006154.

[32] T. Philippe, F. De Geuser, S. Duguay, W. Lefebvre, O. Cojocaru-Mirédin, G. Da Costa, D. Blavette, Clustering and nearest neighbour distances in atom-probe tomography, Ultramicroscopy 109 (10) (2009) 1304–1309, http://dx.doi.org/10.1016/j.ultramic.2009.06.007.

[33] D. Vipin, N. Modi, T. Reynolds, B. Zhang, N. Tabassum, G. Bhowmik, V. Nikas, S. Chakraborty, S. Gallis, M. Huang, Effects of forming gas annealing on luminescence properties of erbium silicate thin films, AIP Adv. 9 (6) (2019) 65018, http://dx.doi.org/10.1063/1.5095953.

[34] G. Wora Adeola, H. Rinnert, P. Miska, M. Vergnat, Influence of the annealing temperature on the photoluminescence of Er-doped SiO thin films, J. Appl. Phys. 102 (5) (2007) 53515, http://dx.doi.org/10.1063/1.2777203.

[35] E. Cattaruzza, M. Back, G. Battaglin, P. Riello, E. Trave, Er-doped alumina crystalline films deposited by radiofrequency magnetron co-sputtering, Opt. Mater. 33 (7) (2011) 1135–1138, http://dx.doi.org/10.1016/j.optmat.2010.10.017.

[36] F. Benz, A. Gonser, R. Völker, T. Walther, J.-T. Mosebach, B. Schwanda, N. Mayer, G. Richter, H.P. Strunk, Concentration quenching of the luminescence from trivalent thulium, terbium, and erbium ions embedded in an AlN matrix, J. Lumin. 145 (2014) 855–858, http://dx.doi.org/10.1016/j.jlumin.2013.09.014.